NJC

Accepted Manuscript

This article can be cited before page numbers have been issued, to do this please use: S. B. Gajera, J. V. Mehta, P. Thakor, V. R. Thakkar, P. Chudasama, J. Patel and M. N. Patel, *New J. Chem.*, 2016, DOI: 10.1039/C6NJ02153K.

ROYAL SOCIETY OF CHEMISTRY

www.rsc.org/njc

View Article Online
DOI: 10.1039/C6NJ02153K

Journal Name

ARTICLE

Half-sandwich iridium^{III} complexes with pyrazole substituted heterocyclic frameworks and its biological applications

Received 00th January 20xx,
Accepted 00th January 20xx

DOI: 10.1039/x0xx00000x

www.rsc.org/

Sanjay B. Gajera,[a] Jugal V. Mehta,[a] Parth Thakor,[b] Vasudev R. Thakkar,[b] Piyushkumar C. Chudasama,[c] Jagdish S. Patel,[c] Mohan N. Patel*[a]

The low-spin Ir^{III} organometallic half-sandwich complexes of type $[(\eta^5\text{-}C_5Me_5)Ir(XY)Cl]^+$, (XY= bipyrazoles (4a-4b)/pyrimidin-2-amines (5a-5b)/triazolo[1,5-a]pyrimidines (6a-6b)) motifs have been synthesized and characterized. All the newly synthesized compounds have been evaluated for DNA binding properties with calf thymus (CT DNA) revealed enhancement in the binding constant (K_b) of complexes. The compounds bearing imidazole substituent are proving a good binder than that of compounds containing phenoxy linkage. Molecular docking attests π-π stacking interactions have been observed between receptor and compounds. Furthermore, the observed DNA cleavage potency has been ascribed to a multitarget mechanism of action of these compounds. Intriguingly, the chelation of ligands with Ir^{III} led to a remarkable enhancement of antibacterial activity against arbitrarily selected two Gram +ve and three Gram –ve bacterial stains. The complexes of triazolo[1,5-a]pyrimidines are proved the most cytotoxic compounds and on *S. pombe* cells compared to pyrazole incorporated heterocyclic frameworks. All complexes showed potent cytotoxicity as compared to ligands, with IC_{50} values ranging from 78 to 234 µM toward A549 human lung cancer cells. Potency of the compounds toward these cancer cells increased with pyrimidin-2-amines > bipyrazole > triazolopyrimidine.

INTRODUCTION

The studies of metal chelates, which bind to DNA strand as reactive models for protein-nucleic acid interaction, provide routes toward rational drug design as well as means to develop sensitive probes for DNA structure and to get information about drug design and tools of molecular biology[1, 2]. Binding of metal complexes with DNA has been studied extensively because DNA is the material of inherence and controls the structure and function of cells[3]. Metal complexes can bind to DNA in a noncovalent interaction mode, such as groove binding for large ligands, electrostatic binding for cations[4], intercalative mode of binding for planar ligands, and partial intercalative binding for incompletely planar ligands[5, 6]. According to the recent reports, cis-platin is one of the most widely used metal-based antitumor and anticancer drugs targeting DNA[7] through covalent bonding interaction[8]. The clinical success of cis-platin, carboplatin, and oxaliplatin[9, 10] have stimulated the search for other transition metal complexes that possess anticancer activity. New metal-based anticancer drugs may be able to widen the spectrum of treatable cancers, reduce toxic side effects, and overcome platinum resistance. Interest in bio-inorganic chemistry and the design of complexes as anticancer agents is currently increasing[11-14]. The cyclopentadienyl ligands can provide hydrophobicity of the faces of the coordination compound (which influences cell uptake and targeting)[15-17]. Most metallodrugs are prodrugs, and control over ligand substitution is vital if the complex is to reach and react with its target site. In this respect, octahedral low-spin d^6 complexes are attractive for drug design since they are often kinetically inert. Inertness increases from the first to second to third row of transition metals[18]. The lifetime for exchange of an aqua ligand on $[Ir(H_2O)_6]^{3+}$, is about 300 years[19, 20]. There are only a limited number of reported studies on the biological activity of iridium complexes. Early studies were concerned with Ir^{I} and Ir^{III} complexes[21, 22] and more recently, a few studies of organometallic Ir^{III} complexes have been reported[23-25]. Iridium^{III} complexes are generally thought to be too inert to possess high reactivity. Indeed, the inertness of Ir^{III} has allowed the design of complexes that function as rigid scaffolds and inhibit kinase enzymes[26]. The biological activity of trans-$[IrCl_4(DMSO)(Im)][ImH]$[27] and trans-$[IrCl_4(Im)_2][ImH]$ (ImH =

[a] Department of Chemistry, Sardar Patel University, Vallabh Vidyanagar-388 120, Gujarat, India.
[b] B. R. Doshi School of Bioscience, Sardar Patel University, Vallabh Vidyanagar-388120, Gujarat, India
[c] Department of Biological Sciences, P. D. Patel Institute of Applied Sciences, CHARUSAT, Changa

Electronic Supplementary Information (ESI) available: [Figures S1–S24 contain the, ^{1}H NMR and ^{13}C NMR (APT) spectrum, S25 is mass spectrum, S26-S33 contains molecular docking images. Table S34 contain DNA cleavage data, Table S35 contain anticancer data, Table 36 MIC data and Table 37 contains cytotoxicity data]. See DOI: 10.1039/x0xx00000x

imidazole)[28], Ir^{III} analogues of the Ru^{III} anticancer drugs NAMI-A and the imidazole analogue of the indazole complex KP1019, respectively, have been attributed to the kinetic inertness of Ir^{III}. The negatively charged pentamethylcyclopentadienyl (Cp*) is an excellent stabilizing ligand for Ir^{III}. In the work reported here, we apply the designed concepts discovered for Ru^{II} and Os^{II} arene complexes to Ir^{III} Cp* complexes $[(\eta^5\text{-Cp*})Ir(XY)Cl]^+$ containing N,N-bound bipyrazole/pyrimidin-2-amine/triazolopyrimidine as chelating ligands. Only a few iridium complexes containing functionalized Cp* ligands have been reported previously. We have studied the effect of functionalization of ligand interaction with DNA, molecular docking, anticancer activity on A549, antibacterial and cytotoxicity on *S. Pombe* cells and brine shrimp lethality assay. Such complexes can be thermodynamically stable and yet kinetically labile toward substitution reactions and that substituents on chelating ligand can have a dramatic effect on chemical and biological activities.

EXPERIMENTAL SECTION

Materials and Reagents

All reagents and solvents were purchased commercially and used without further purification unless otherwise noted. The purity of compounds was assessed by different analytical techniques like ESI mass, LC-MS, CHN analysis, ^{1}H NMR, ^{13}C NMR and IR spectra. The measured molecular weights of ligands (intermediates) as well as complexes were consistent with expected values which permitted unambiguous identification and assessment of purity. $iridium^{III}$ dimer, guanidine hydrochloride, 3-amino-1, 2, 4-triazole and potassium tert-butoxide were purchased from Sigma-Aldrich. Agarose, Luria broth, ethidium bromide and tris(hydroxymethyl) methylamine (tris-HCl) were purchased from Hi-media Laboratories Pvt. Ltd., India. Culture of pUC19 (MTCC 47), *Staphylococcus aureus (S. aureus)* (MTCC–3160), *Bacillus subtilis (B. subtilis)* (MTCC–7193), *Serratia marcescens (S. marcescens)* (MTCC–7103), *Pseudomonas aeruginosa (P. aeruginosa)* (MTCC–1688) and *Escherichia coli (E. coli)* (MTCC– 433) were purchased from the Institute of Microbial Technology (Chandigarh, India).

Cell lines and culture conditions

The lung carcinoma cell line (A549) was procured from NCCS, Pune, India. The passage number of 19-25 was used in the present study. Apart from this the cell line was maintained as a monolayer in DMEM/F12 (Gibco, Invitrogen, CA, USA) containing 10% foetal bovine serum (Gibco, Invitrogen, CA, USA) supplemented with 50 U/mL penicillin, 50 µg/mL streptomycin at 37˚C in a humidified atmosphere of 5% CO_2/ 95% air.

Analytical measurements

NMR spectroscopy

^{1}H NMR and ^{13}C NMR spectra were obtained in 5 mm NMR tubes at 298 K (unless stated otherwise) on Bruker Avance (400 MHz) spectrometers. ^{1}H NMR chemical shifts were internally referenced to $(CHD_2)(CD_3)SO$ (2.50 ppm) for DMSO-d_6 and $CDCl_3$ (7.26 ppm) for chloroform-d_1. ^{13}C NMR chemical shifts were internally referenced to $CDCl_3$ (77.16 ppm) for chloroform-d_1 and $(CD_3)_2SO$ (39.52 ppm) for DMSO-d_6.

Mass spectrometry

Electrospray ionization mass spectra were obtained by infusing into the mass spectrometer (LC-MS Spectrometer Model Q-ToF Micro Waters). The mass spectra were recorded with a scan range of m/z 50-1000 for positive ions.

Elemental analysis

All biologically evaluated compounds synthesized within this report have been analysed using elemental (CHN) analysis by means of combustion. This technique requires the sample to be burned in an excess of oxygen and has a variety of traps which collect the combustion products: CO_2, H_2O, and NO. These masses are then used to help calculate the masses of the unknown product. The experimental values are compared with the calculated values of the sample. Thermo finnigan elemental analyzer was used to analyse carbon, hydrogen and nitrogen content of the compounds.

UV-Vis spectroscopy

UV–160A UV–Vis spectrophotometer was used with 1 cm path length quartz cuvettes (2.5 mL). Spectra were processed using UV-probe software. Experiments were carried out at 298 K unless otherwise stated.

Synthesis of 5-(*1H*-imidazol-1-yl)-3-methyl-1-phenyl-1H-pyrazole-4-carbaldehyde (1a)

5-Chloro-3-methyl-1-phenyl-*1H*-pyrazole-4-carbaldehyde (1 mmol), imidazole (1 mmol) and anhydrous potassium carbonate (2 mmol) in dimethyl formamide (10 mL) were charged in a 100 mL round bottom flask equipped with a mechanical stirrer and a condenser. The reaction mixture was heated at 90 ºC for 2 h. The progress of the reaction was monitored by TLC. After the completion of reaction as confirmed by TLC, the reaction mixture was poured into 100 mL ice-water, filtered, washed thoroughly with water, dried and recrystallized from ethanol to obtain a white solid.

Synthesis of 3-methyl-5-phenoxy-1-phenyl-*1H*-pyrazole-4-carbaldehyde (1b)

5-Chloro-3-methyl-1-phenyl-*1H*-pyrazole-4-carbaldehyde (1 mmol), phenol (1 mmol) and anhydrous potassium carbonate (2 mmol) in dimethyl formamide (10 mL) were charged in a 100 mL round bottom flask equipped with a mechanical stirrer and a condenser. The reaction mixture was heated at 90 ºC for 2 h. The progress of the reaction was monitored by TLC. After the completion of reaction as confirmed by TLC, the reaction mixture was poured in to 100 mL ice-water, filtered, washed thoroughly with water, dried and recrystallized from ethanol to obtain a white solid.

Synthesis of (*E*)-3-(5-(1H-imidazol-1-yl)-3-methyl-1-phenyl-*1H*-pyrazol-4-yl)-1-(pyridin-2-yl)prop-2-en-1-one (3a)

To a mixture of 5-(*1H*-imidazol-1-yl)-3-methyl-1-phenyl-*1H*-pyrazole-4-carbaldehyde (1a) (5.0 mmol), 2- acetyl pyridine (5.0 mmol) and 20% ethanolic NaOH (5 mL) were added. The reaction mixture was stirred at room temperature until formation of precipitate. The obtained product was isolated by

filtration, washed with cold ethanol and recrystallized from $CHCl_3$.

Synthesis of (*E*)-3-(3-methyl-5-phenoxy-1-phenyl-*1H*-pyrazol-4-yl)-1-(pyridin-2-yl)prop-2-en-1-one (3b)

To a mixture of 3-methyl-5-phenoxy-1-phenyl-*1H*-pyrazole-4-carbaldehyde (1b) (5.0 mmol), 2- acetyl pyridine (5.0 mmol) and 20% ethanolic NaOH (5 mL) were added. The reaction mixture was stirred at room temperature until formation of precipitate. The obtained product was isolated by filtration, washed with cold ethanol and recrystallized from $CHCl_3$.

5'-(*1H*-Imidazol-1-yl)-3'-methyl-1',2-diphenyl-5-(pyridin-2-yl)-3,4-dihydro-*1'H,2H*-3,4'-bipyrazole (bpy-N) [4a]

(*E*)-3-(5-(*1H*-Imidazol-1-yl)-3-methyl-1-phenyl-*1H*-pyrazol-4-yl)-1-(pyridin-2-yl)prop-2-en-1-one (3a) (1.0 mmol) and phenyl hydrazine (1.0 mmol) were thoroughly mixed in ethanol (5 mL) with catalytic amount of potassium tertiary butoxide in a 50 mL round bottom flask. The reaction mixture was refluxed for 5 hrs. After the completion of the reaction as monitored by TLC (ethyl acetate: hexane: 1:5), the reaction mixture was cooled to room temperature washed with water and dried over Na_2SO_4. The ensuing product upon purification by chromatography experiment (silica gel 60–120 mesh, eluent 20% EtOAc/hexanes) gave the desired compound as a white solid) (scheme 1). Yield: 79 %; M.p. 259 °C; Mol wt.: 445.53 gm/mol; LC-MS (*m/z*): 446 (M^+); Elemental analysis (%): calc. for $C_{27}H_{23}N_7$: C, 72.79; H, 5.20; N, 22.01. Found: C, 72.85; H, 5.15; N, 22.05; IR (KBr, υ_{max}, cm^{-1}): 2924 (aromatic ring –CH stretching), 1597 (–C═N), 1498 (-CH_2 scissoring), 1388 (–CH_3 rocking); 1246 (C-N), 756 (-CH bending), ^{1}H NMR (400 MHz, $CHCl_3$-d_1): δ (ppm) 2.356 (s, 3H, CH_3), 3.434 (dd, 1H, J = 7.2 Hz, 18 Hz, C_4-H_a of pyrazoline), 3.918 (dd, 1H, J = 13.2 Hz, 18.0 Hz, C_4-H_b of pyrazoline), 5.240 (dd, 1H, J = 7.2 Hz, 12.8 Hz, C_5-H of pyrazoline), 6.788–8.557 (m, 17H, Ar–H); ^{13}C{^{1}H} NMR (100 MHz, $CHCl_3$-d_1): δ (ppm) 13.13 (-CH_3 of pyrazole), 41.25 (-CH of pyrazoline), 54.67 (-CH_2 of pyrazoline), 117.03, 131.98, 137.92, 143.58, 147.15, 147.87, 151.71 (C of aromatic); 113.55, , 120.18, 120.59, 120.65, 122.39, 122.86, 127.85, 129.11, 129.34, 130.53, 136.03, 137.41, 149.05 (CH of aromatic).

3'-Methyl-5'-phenoxy-1',2-diphenyl-5-(pyridin-2-yl)-3,4-dihydro-*1'H,2H*-3,4'-bipyrazole (bpy-O) [4b]

The synthesis was performed as for 4a using (*E*)-3-(3-methyl-5-phenoxy-1-phenyl-*1H*-pyrazol-4-yl)-1-(pyridin-2-yl)prop-2-en-1-one (3b) (1.0 mmol) and phenyl hydrazine (1.0 mmol). Yield: 75 %; M.p.: 249 °C; Mol wt.: 471.56 gm/mol; LC-MS (*m/z*): 472 (M^+); Elemental analysis (%): calc. for $C_{30}H_{25}N_5O$: C, 76.41; H, 5.34; N, 14.85. Found: C, 76.55; H, 5.43; N, 14.90; IR (KBr, υ_{max}, cm^{-1}): 2924 (aromatic ring –CH stretching), 1597 (–C═N), 1504 (-CH_2 scissoring), 1389 (–CH_3 rocking); 1246 (C-N), 995 (C-O-C) 771 (-CH bending), ^{1}H NMR (400 MHz, DMSO-d_6): δ (ppm) 2.196 (s, 3H, CH_3), 3.405 (dd, 1H, J = 7.2 Hz, 18.4 Hz, C_4-H_a of pyrazoline), 4.070 (dd, 1H, J = 13.2 Hz, 18.0 Hz, C_4-H_b of pyrazoline), 5.643 (dd, 1H, J = 6.8 Hz, 13.2 Hz, C_5-H of pyrazoline), 6.894–8.705 (m, 19H, Ar–H); ^{13}C{^{1}H} NMR (100 MHz, DMSO-d_6): δ (ppm) 12.33 (-CH_3 of pyrazole), 42.25 (-CH_2 of pyrazoline), 54.57 (-CH of pyrazoline); 117.03, 124.67, 132.88, 137.11, 143.98, 147.15, 147.17, 151.81 (C of aromatic); 114.50, 121.38, 121.52, 121.63, 123.37, 123.76, 128.85, 130.11, 130.32, 131.55, 136.03, 137.42, 149.55 (CH of aromatic).

4-(5-(*1H*-Imidazol-1-yl)-3-methyl-1-phenyl-*1H*-pyrazol-4-yl)-6-(pyridin-2-yl)pyrimidin-2-amine (pma-N) [5a]

(*E*)-3-(5-(*1H*-Imidazol-1-yl)-3-methyl-1-phenyl-*1H*-pyrazol-4-yl)-1-(pyridin-2-yl)prop-2-en-1-one (3a) (1.0 mmol) and guanidine hydrochloride (1.0 mmol) were thoroughly mixed in ethanol (5 mL) with catalytic amount of potassium tertiary butoxide in a 50 mL round bottom flask. The reaction mixture was refluxed for 6 hrs. After the completion of the reaction as monitored by TLC (ethyl acetate: hexane: 1:5), the reaction mixture was cooled to room temperature washed with water and dried over Na2SO4. The ensuing product upon purification by chromatography experiment (silica gel 60–120 mesh, eluent 20% EtOAc/hexanes) gave the desired compound as a white solid (scheme 1). Yield: 79 %; M.p.: 250 °C; Mol wt.: 394.44 gm/mol; LC-MS (*m/z*): 395 (M^+); Elemental analysis (%): calc. for $C_{22}H_{18}N_8$: C, 66.99; H, 4.60; N, 28.41. Found: C, 66.85; H, 4.53; N, 28.45; IR (KBr, υ_{max}, cm^{-1}): 3309 (-NH_2), 2924 (aromatic ring –CH stretching), 1581 (–C═N), 1373 (–CH_3 rocking); 1231 (C-N), 763 (-CH bending); ^{1}H NMR (400 MHz, $CHCl_3$-d_1): δ (ppm) 2.379 (s, 3H, CH_3), 5.230 (s, 2H, NH_2), 6.940–7.670 (m, 13H, Ar–H); ^{13}C{^{1}H} NMR (100 MHz, $CHCl_3$-d_1): δ (ppm) 12.86 (-CH_3 of pyrazole); 120.19, 127.67, 128.35, 132.15, 136.57, 136.91, 137.65, 148.32 (C of aromatic); 119.07, 121.25, 122.69, 123.06, 125.02, 129.29, 129.91, 136.09, 138.55, 148.38, 149.53 (CH of aromatic).

4-(3-Methyl-5-phenoxy-1-phenyl-*1H*-pyrazol-4-yl)-6-(pyridin-2-yl)pyrimidin-2-amine (pma-O) [5b]

The synthesis was performed as for 5a using (*E*)-3-(3-methyl-5-phenoxy-1-phenyl-*1H*-pyrazol-4-yl)-1-(pyridin-2-yl)prop-2-en-1-one (3b) (1.0 mmol) and guanidine hydrochloride (1.0 mmol). Yield: 79 %; M.p.: 249 °C; Mol wt.: 420.48 gm/mol; LC-MS (m/z): 421 (M+); Elemental analysis (%): calc. for $C_{25}H_{20}N_6O$: C, 71.41; H, 4.79; N, 19.99; Found: C, 71.45; H, 4.85; N, 19.95; IR (KBr, υmax, cm-1): 3303 (-NH_2), 2924 (aromatic ring –CH stretching), 1574 (–C═N), 1381 (–CH_3 rocking), 1202 (-C-N), 1033 (C-O-C), 756 (-CH bending); ^{1}H NMR (400 MHz, $CHCl_3$-d_1): δ (ppm) 2.360 (s, 3H, CH_3), 5.239 (s, 2H, NH_2), 6.857–7.641 (m, 15H, Ar–H); ^{13}C{^{1}H} NMR (100 MHz, $CHCl_3$-d^1): δ (ppm) 13.58 (-CH_3 of pyrazole); 111.04, 115.26, 115.62, 119.10, 136.41, 138.04, 145.34, 148.41, 157.22 (C of aromatic); 122.04, 122.70, 122.83, 123.19, 123.40, 126.64, 129.00, 129.12, 129.67, 129.77, 148.69 (CH of aromatic).

7-(5-(*1H*-Imidazol-1-yl)-3-methyl-1-phenyl-*1H*-pyrazol-4-yl)-5-(pyridin-2-yl)-[1,2,4]triazolo[1,5-a]pyrimidine (tpm-N) [6a]

An oven dried 25 mL RB flask was charged with (*E*)-3-(5-(*1H*-Imidazol-1-yl)-3-methyl-1-phenyl-*1H*-pyrazol-4-yl)-1-(pyridin-2-yl)prop-2-en-1-one (3a) (1.0 mmol), 3- aminotriazole (1.2 mmol), KOH (0.1 mmol) and DMF (5 mL). The resulting solution was stirred at 110 ^{0}C for 20 min. On completion, the reaction mass was allowed to cool to ambient temperature, diluted with water (20 mL) and extracted into ethyl acetate (2 x 20 mL). The combined organic layers were dried over anhydrous Na_2SO_4, and organic solvent was evaporated on a rotatory evaporator.

View Article Online
DOI: 10.1039/C6NJ02153K

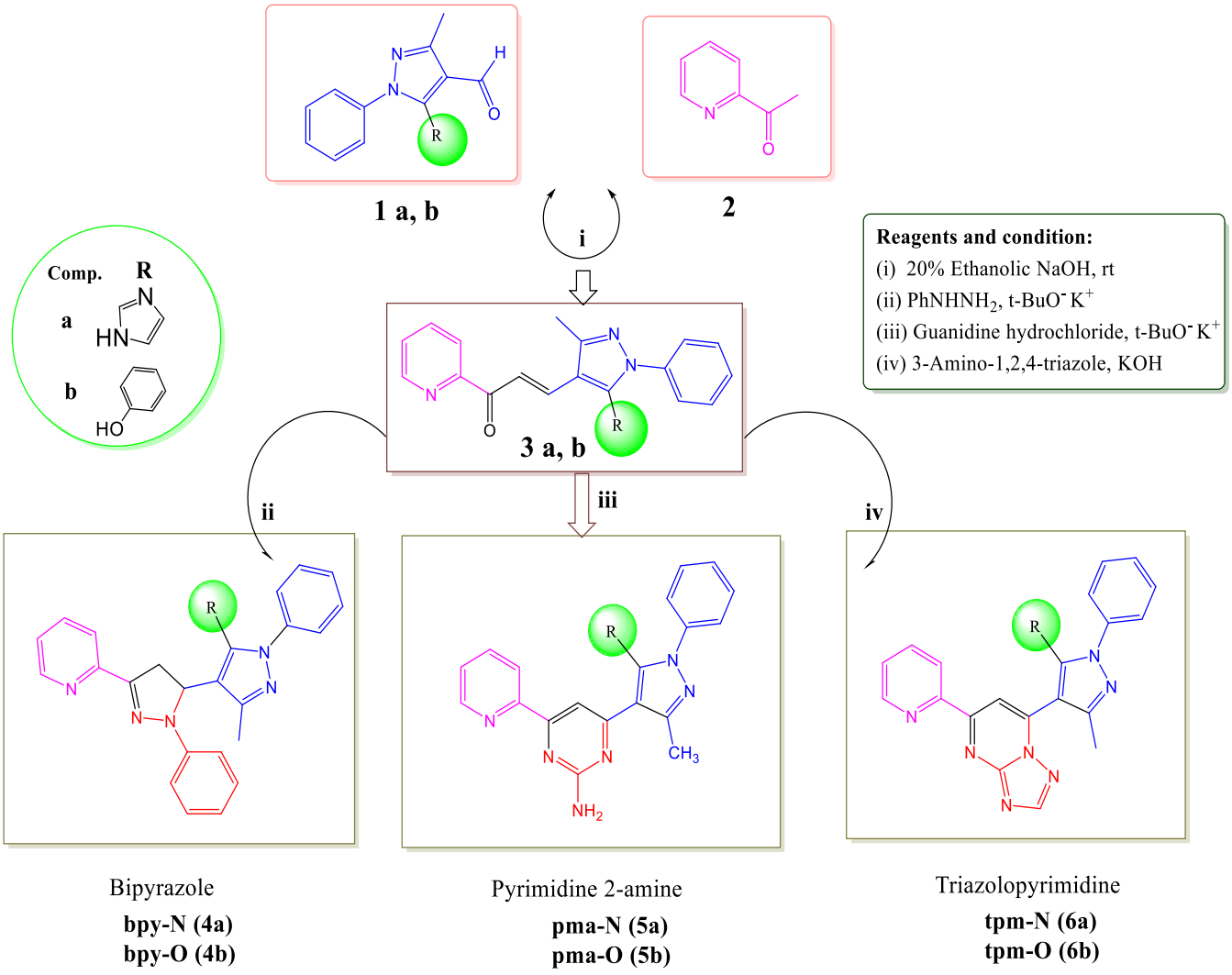

Preparation of three different prototypes from a common scaffold of chalcone

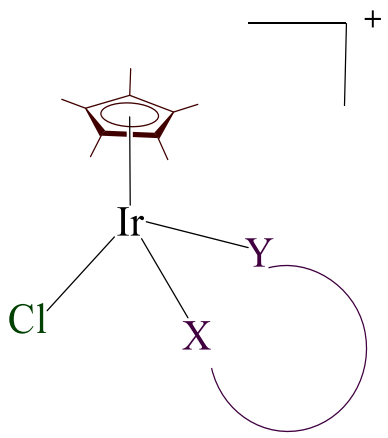

Complex	XY
7 a, b	Bipyrazole
8 a, b	Pyrimidin-2-amine
9 a, b	Triazolopyrimidine

Scheme 1: Synthesis of bipyrazole, pyrimidin-2-amine, triazolopyrimidine and Ir^{III} complexes

View Article Online
DOI: 10.1039/C6NJ02153K

The crude residue was purified by chromatography experiment (silica gel 60–120 mesh, eluent 20% EtOAc/hexanes) affording compounds 6a (scheme 1). Yield: 75 %; M.p.: 241 °C; Mol wt.: 419.45 gm/mol; LC-MS (*m/z*): 419 (M^+); Elemental analysis (%): calc. for $C_{23}H_{17}N_9$: C, 65.86; H, 4.09; N, 30.05. Found: C, 65.79; H, 4.15; N, 30.11; IR (KBr, υ_{max}, cm^{-1}): 2916 (aromatic ring –CH stretching), 1558 (–C═N), 1381 ($–CH_3$ rocking); 1203 (C-N), 756 (-CH bending); ^1H NMR (400 MHz, DMSO-d_6): δ (ppm) 2.348 (s, 3H, CH_3), 7.243–9.310 (m, 14H, Ar–H); $^{13}C\{^1H\}$ NMR (100 MHz,DMSO-d_6): δ (ppm) 14.65 ($-CH_3$ of pyrazole); 110.29, 123.53, 133.69, 137.58, 144.29, 149.91, 153.21, 159.73 (C of aromatic); 109.13, 118.34, 120.89, 121.63, 125.60, 126.02, 127.01, 134.52, 143.13, 150.32, 155.85, 156.84 (CH of aromatic).

7-(3-Methyl-5-phenoxy-1-phenyl-*1H*-pyrazol-4-yl)-5-(pyridin-2-yl)-[1,2,4]triazolo[1,5-a]pyrimidine (tpm-O) [6b]

The synthesis was performed as for 6a using (*E*)-3-(3-methyl-5-phenoxy-1-phenyl-*1H*-pyrazol-4-yl)-1-(pyridin-2-yl)prop-2-en-1-one (3b) (1.0 mmol), 3-aminotriazole (1.2 mmol), KOH (0.1 mmol) and DMF (5 mL). Yield: 75 %; M.p.: 236 °C; Mol wt.: 445.49 gm/mol; LC-MS (*m/z*): 446 (M^+); Elemental analysis (%): calc. for $C_{26}H_{19}N_7O$: C, 70.10; H, 4.30; N, 22.01; Found: C, 70.05; H, 4.15; N, 22.08; IR (KBr, υ_{max}, cm^{-1}): 2931 (aromatic ring –CH stretching), 1551 (–C═N), 1381 ($–CH_3$ rocking), 1235 (-C-N), 995 (C-O-C), 763 (-CH bending); ^1H NMR (400 MHz, DMSO-d_6): δ (ppm) 2.421 (s, 3H, CH_3), 7.194–9.211 (m, 16H, Ar–H); $^{13}C\{^1H\}$ NMR (100 MHz, DMSO-d_6): δ (ppm) 12.15 ($-CH_3$ of pyrazole); 110.39, 123.57, 132.15, 133.69, 137.58, 144.16, 149.91, 153.28, 159.71 (C of aromatic); 108.18, 117.34, 120.39, 121.63, 124.64, 125.06, 126.01, 134.52, 143.13, 150.32, 155.85, 156.64 (CH of aromatic).

Synthesis of $[(\eta^5\text{-}C_5Me_5)Ir(bpy\text{-}N)Cl]Cl$ [7a]

A solution of $[(\eta^5\text{-}C_5Me_5)\text{-}IrCl_2]_2$ (0.06 mmol) and bipyrazole (4a) (0.12 mmol) in CH_2Cl_2 (15 mL) was stirred for 2 h at ambient temperature. The solution was filtered through Celite. The filtrate was evaporated to dryness on a rotary evaporator and washed with diethyl ether. The product was recrystallized from $CHCl_3$/hexane (scheme 1). Yield: 70 %; M.p.: > 300 °C; Mol wt.: 843.88 gm/mol; MS (ESI, m/z): 809 $[M\text{-}Cl]^+$; Ω_M: 69 Ω^{-1} cm^2 mol^{-1}; Elemental analysis (%): calc. for $C_{37}H_{38}N_7Cl_2Ir$: C, 52.66; H, 4.54; N, 11.62; Ir, 22.78; Found: C, 52.76; H, 4.56; N, 11.66; Ir, 22.82; IR (KBr, υ_{max}, cm^{-1}): 2916 (aromatic ring –CH stretching), 1597 (–C═N), 1499 ($-CH_2$ scissoring), 1389 ($–CH_3$ rocking); 1248 (C-N), 763 (-CH bending); ^1H NMR (400 MHz, DMSO-d_6): δ (ppm) = 1.370 (s, 15H, Cp* CH_3) 2.547 (s, 3H, CH_3), 3.984 (dd, 1H, J = 17.6 Hz, 30 Hz, C_4-H_a of pyrazoline), 4.321 (dd, 1H, J = 14.8 Hz, 30.0 Hz, C_4-H_b of pyrazoline), 5.079 (dd, 1H, J = 11.6 Hz, 23.6 Hz, C_5-H of pyrazoline), 7.073–8.967 (m, 17H, Ar–H); $^{13}C\{^1H\}$ NMR (100 MHz, DMSO-d_6): δ (ppm) 8.65 (Cp*-CH_3), 15.08 ($-CH_3$ of pyrazole), 43.58 ($-CH_2$ of pyrazoline) 53.53 (-CH of pyrazoline), 90.08 (Cp*-C); 113.55, 120.65, 142.98, 148.03, 149.41, 150.92, 153.58 (C of aromatic); 117.03, 120.18, 120.59, 122.39, 122.86, 125.02, 125.44, 129.56, 129.81, 137.85, 139.11, 139.34, 140.53 (CH of aromatic).

Synthesis of $[(\eta^5\text{-}C_5Me_5)Ir(bpy\text{-}O)Cl]Cl$ [7b]

The synthesis was performed as for 7a using $[(\eta^5\text{-}C_5Me_5)\text{-}IrCl_2]_2$ (0.06 mmol) and bipyrazole (4b) (0.12 mmol). Yield: 65 %; M.p.: > 300 °C; Mol wt.: 869.91 gm/mol; MS (ESI, m/z): 834 $[M\text{-}Cl]^+$; Ω_M: 72 Ω^{-1} cm^2 mol^{-1}; Elemental analysis (%): calc. for $C_{40}H_{40}N_5OCl_2Ir$: C, 55.23; H, 4.63; N, 8.05; Ir, 22.10; Found: C, 55.20; H, 4.56; N, 8.10; Ir, 22.16; IR (KBr, υ_{max}, cm^{-1}): 2916 (aromatic ring –CH stretching), 1597 (–C═N), 1497 ($-CH_2$ scissoring), 1381 ($–CH_3$ rocking); 1249 (C-N), 1026 (C-O-C), 772 (-CH bending); ^1H NMR (400 MHz, DMSO-d_6): δ (ppm) = 1.373 (s, 15H, Cp* CH_3), 2.251 (s, 3H, CH_3), 3.989 (dd, 1H, J = 17.6 Hz, 30 Hz, C_4-H_a of pyrazoline), 4.331 (dd, 1H, J = 14.8 Hz, 30.0 Hz, C_4-H_b of pyrazoline), 5.099 (dd, 1H, J = 11.6 Hz, 23.6 Hz, C_5-H of pyrazoline), 7.082–8.921 (m, 19H, Ar–H); $^{13}C\{^1H\}$ NMR (100 MHz, DMSO-d_6): δ (ppm) 8.73 (Cp*-CH_3), 13.32 ($-CH_3$ of pyrazole), 42.15 ($-CH_2$ of pyrazoline), 53.38 (-CH of pyrazoline), 89.98 (Cp*-C); 120.19, 122.69, 123.06, 148.32, 148.38, 149.53, 150.93, 151.24 (C of aromatic); 119.07, 121.25, 125.02, 127.67, 128.35, 129.29, 129.91, 132.15, 136.09, 136.57, 136.91, 137.65, 138.55 (CH of aromatic).

Synthesis of $[(\eta^5\text{-}C_5Me_5)Ir(pma\text{-}N)Cl]Cl$ [8a]

The synthesis was performed as for 7a using $[(\eta^5\text{-}C_5Me_5)\text{-}IrCl_2]_2$ (0.06 mmol) and pyrimidin-2-amine (5a) (0.12 mmol). Yield: 69 %; M.p.: > 300 °C; Mol wt.: 792.79 gm/mol; MS (ESI, m/z): 757 $[M\text{-}Cl]^+$; Ω_M: 65 Ω^{-1} cm^2 mol^{-1}; Elemental analysis (%): calc. for $C_{32}H_{33}N_8Cl_2Ir$: C, 48.48; H, 4.20; N, 14.13; Ir, 24.25; Found: C, 48.42; H, 4.26; N, 14.22; Ir, 24.30; IR (KBr, υ_{max}, cm^{-1}): 3351 ($-NH_2$), 2916 (aromatic ring –CH stretching), 1597 (–C═N), 1381 ($–CH_3$ rocking); 1250 (C-N), 771 (-CH bending); ^1H NMR (400 MHz, DMSO-d_6): δ (ppm) = 1.542 (s, 15H, Cp* CH_3), 2.306 (s, 3H, CH_3), 5.609 (s, 2H, NH_2), 6.992–8.569 (m, 13H, Ar–H); $^{13}C\{^1H\}$ NMR (100 MHz, DMSO-d_6): δ (ppm) 8.89 (Cp*-CH_3), 14.44 ($-CH_3$ of pyrazole), 87.69 (Cp*-C); 108.50, 130.64, 137.94, 148.08, 148.98, 155.86, 155.98, 156.77 (C of aromatic); 115.37, 116.01, 122.20, 122.30, 123.87, 124.22, 126.99, 127.59, 129.73, 129.83, 139.55 (CH of aromatic).

Synthesis of $[(\eta^5\text{-}C_5Me_5)Ir(pma\text{-}O)Cl]Cl$ [8b]

The synthesis was performed as for 7a using $[(\eta^5\text{-}C_5Me_5)\text{-}IrCl_2]_2$ (0.06 mmol) and pyrimidin-2-amine (5b) (0.12 mmol). Yield: 71 %; M.p.: > 300 °C; Mol wt.: 818.82 gm/mol; MS (ESI, m/z): 783 $[M\text{-}Cl]^+$; Ω_M: 66 Ω^{-1} cm^2 mol^{-1}; Elemental analysis (%): calc. for $C_{35}H_{35}N_6OCl_2Ir$: C, 51.34; H, 4.31; N, 10.26; Ir, 23.47; Found: C, 51.44; H, 4.37; N, 10.36; Ir, 23.55; IR (KBr, υ_{max}, cm^{-1}): 3417 ($-NH_2$), 2916 (aromatic ring –CH stretching), 1550 (–C═N), 1381 ($–CH_3$ rocking), 1196 (-C-N), 1026 (C-O-C), 763 (-CH bending); ^1H NMR (400 MHz, DMSO-d_6): δ (ppm) = 1.542 (s, 15H, Cp* CH_3), 2.306 (s, 3H, CH_3), 5.622 (s, 2H, NH_2), 6.732–9.005 (m, 15H, Ar–H); $^{13}C\{^1H\}$ NMR (100 MHz, DMSO-d_6): δ (ppm) 9.89 (Cp*-CH_3), 14.49 ($-CH_3$ of pyrazole), 89.69 (Cp*-C); 109.50, 130.64, 136.94, 148.08, 148.98, 158.06, 159.08, 162.57, 163.98 (C of aromatic); 115.37, 116.01, 122.00, 122.30, 123.87, 124.02, 126.99, 127.99, 129.73, 129.89, 138.55 (CH of aromatic).

Synthesis of $[(\eta^5\text{-}C_5Me_5)Ir(tpm\text{-}N)Cl]Cl$ [9a]

The synthesis was performed as for 7a using $[(\eta^5\text{-}C_5Me_5)\text{-}IrCl_2]_2$ (0.06 mmol) and triazolopyrimidine (6a) (0.12 mmol). Yield: 75

View Article Online
DOI: 10.1039/C6NJ02457K

%; M.p.: > 300 °C; Mol wt.: 817.80 gm/mol; MS (ESI, m/z): 782 $[M\text{-}Cl]^+$; Ω_M: 62 Ω^{-1} cm^2 mol^{-1}; Elemental analysis (%): calc. for $C_{33}H_{32}N_9Cl_2Ir$: C, 48.47; H, 3.94; N, 15.41; Ir, 23.50; Found: C, 48.56; H, 3.90; N, 15.39; Ir, 23.59; IR (KBr, υ_{max}, cm^{-1}): 2916 (aromatic ring –CH stretching), 1558 (–C═N), 1381 ($–CH_3$ rocking); 1204 (C-N), 764 (-CH bending); ^1H NMR (400 MHz, DMSO-d_6): δ (ppm) = 1.774 (s, 15H, Cp* CH_3), 2.483 (s, 3H, CH_3), 7.622–9.201 (m, 14H, Ar–H); $^{13}C\{^1H\}$ NMR (100 MHz, DMSO-d_6): δ (ppm) 9.65 (Cp*-CH_3), 14.51 (-CH_3 of pyrazole), 91.15 (Cp*-C); 112.35, 130.21, 137.43, 143.55, 159.86, 165.22, 165.81, 166.93 (C of aromatic); 113.13, 124.01, 125.90, 127.86, 129.82, 131.23, 139.55, 141.27, 150.45, 153.27, 153.74, 154.53 (CH of aromatic).

Synthesis of $[(\eta^5\text{-}C_5Me_5)Ir(tpm\text{-}O)Cl]Cl$ [9b]

The synthesis was performed as for 7a using $[(\eta^5\text{-}C_5Me_5)\text{-}IrCl_2]_2$ (0.06 mmol) and triazolopyrimidine (6b) (0.12 mmol). Yield: 73 %; M.p.: > 300 °C; Mol wt.: 843.83 gm/mol; MS (ESI, m/z): 808 $[M\text{-}Cl]^+$; Ω_M: 64 Ω^{-1} cm^2 mol^{-1}; Elemental analysis (%): calc. for $C_{36}H_{34}N_7OCl_2Ir$: C, 51.24; H, 4.06; N, 11.62; Ir, 22.78; Found: C, 51.14; H, 4.00; N, 11.56; Ir, 22.85; IR (KBr, υ_{max}, cm^{-1}): 2916 (aromatic ring –CH stretching), 1558 (–C═N), 1381 ($–CH_3$ rocking), 1252 (-C-N), 1026 (C-O-C), 764 (-CH bending); ^1H NMR (400 MHz, DMSO-d_6): δ (ppm) = 1.775 (s, 15H, Cp* CH_3), 2.578 (s, 3H, CH_3), 7.626–9.411 (m, 16H, Ar–H); $^{13}C\{^1H\}$ NMR (100 MHz, DMSO-d_6): δ (ppm) 8.86 (Cp*-CH_3), 14.21 (-CH_3 of pyrazole), 90.05 (Cp*-C); 114.85, 128.84, 137.59, 141.13, 154.95, 161.13, 161.75, 162.43, 150.70 (C of aromatic); 106.88, 116.09, 121.32, 125.83, 125.96, 126.06, 129.77, 129.95, 130.21, 130.64, 149.96, 153.33 (CH of aromatic).

Absorption spectroscopy in the presence of CT-DNA

The absorption spectra were recorded on a Shimadzu UV-2450 UV-Vis spectrophotometer using cuvettes of 1 cm path length. Absorption spectral titration experiments were performed by maintaining a constant concentration of the complex and varying the nucleic acid concentration. It was achieved by dissolving an appropriate amount of the metal complex, DNA stock solutions and maintaining the total volume constant. The absorbance (A) of the most red-shifted band of each complex was recorded after successive additions of CT DNA. The stock solution was prepared by dissolving CT-DNA in a Tris HCl buffer (pH 7.2) and kept overnight at 4 °C for complete dissolution. The DNA concentration per nucleotide was determined by absorption spectroscopy using the molar absorption coefficient (6600 M^{-1} cm^{-1}) at 260 nm[29, 30].

Molecular docking of the complexes with the DNA duplex with sequence $d(CGCGAATTCGCG)_2$

AutoDock vina was used for the prediction of binding affinity and searching for the optimum binding site together with the AutoDock Tools (ADT) to set up and perform blind docking calculations of all compounds binding to CT-DNA. Since CT-DNA used in the experimental work was too large for current computational resources to perform the dock calculation, the structure of the DNA with sequence $d(CGCGAATTCGCG)_2$ (PDB id: 1BNA, a familiar sequence) obtained from the Protein Data Bank (www.rcsb.org/pdb). The receptor (CT-DNA) and the ligand (iridium^{III} and pyrazole incorporated ligands) files were prepared using AutoDock Tools. The hetero atoms including water molecules were deleted, polar hydrogen atoms and Kollman charges were added to the receptor molecule. All other bonds were allowed to be rotatable. In the docking analysis, the binding site was assigned across all of the minor and major grooves of the DNA molecule, which was enclosed in a box with the number of grid points in x × y × z directions, 60 × 74 × 116 and a grid spacing of 0.375 Å. All calculations were performed on an Intel Core i3 based machine running windows 7 operating system. For each of the docking cases, the lowest energy docked conformation, according to the AutoDock scoring function, was selected as the binding mode[31]. Visualization of the docked pose was done by using AutoDock 1.5.6[31].

Chemical nuclease activity

The DNA cleavage study was performed using pUC19 DNA with synthesized compounds. The samples were incubated for 1 h at 37°C. The samples were analysed by 1% agarose gel electrophoresis [Tris–acetate–ethylenediaminetetraacetic acid, (TAE) buffer, pH 8.0] for 3 h. at 100 mV. The gel was stained with (0.5 mg mL^{-1}) ethidium bromide. The gels were viewed in an Alpha Innotech Corporation Gel doc system and photographed using a CCD camera. The cleavage efficiency was measured by determining the ability of the complex to convert the supercoiled DNA (SC) to nicked circular (NC) and linear forms (L).

Antiproliferative study

The 10,000 cells/well were seeded in 96 well culture plates and allow to grow for 24 h. After 24 h. cells were treated with the various concentrations of synthesized compounds dissolved in molecular grade of DMSO to find out appropriate IC_{50} value of the respective compounds. Next day, 10 µL of tetrazolium dye (MTT) (5 mg/mL) was added to each well and incubated for 3-4 h. in CO_2 incubator at 37°C. Volume of culture was 100 µL in each well. After the incubation period, the culture medium was removed and the purple crystals formed were dissolved in 100 µL of molecular grade DMSO. The absorbance was recorded with the help of micro plate reader at 570 nm.

In vitro antibacterial activity

The minimal inhibitory concentrations (MIC) were tested against three Gram-negative microorganisms namely *Escherichia coli* (MTCC 433), *Pseudomonas aeruginosa* (MTCC P-09), *Serratia marcescens* (MTCC 7103) and two Gram-positive bacteria namely *Bacillus subtilis* (MTCC 7193) and *Staphylococcus aureus* (MTCC 3160). The antibacterial activity for the test compounds was performed to determine the bacteriostatic concentration, i.e. minimal inhibitory concentration (MIC). The MIC value was determined by two fold serial dilution technique in triplicates. The lowest compound concentration inhibiting visible bacterial growth is reported as MIC[32, 33].

In vitro cytotoxicity bioassay

View Article Online
DOI: 10.1039/C6NJ02157K

The cytotoxicity assay was performed on brine shrimp nauplii using Meyer method. The lethal concentrations of compounds resulting in 50% mortality (LC_{50}) of the brine shrimp from the 24 h and the dose–response data were transformed into a straight line by means of a trend line fit linear regression analysis; the LC_{50} was determine from the best-fit line obtained by plotting % mortality *vs.* concentration. All data has been collected from at least three independent experiments and the LC_{50} determined using OriginPro 8 software as previously described[34-36].

Cellular level cytotoxicity

Due to eukaryotic and fairly big size characteristics of *S. pombe*, it is become an important tool to study cell biology. Cytotoxicity of synthesized compounds was tested using bioassay on *S. pombe* cells at the cellular level as previously described[37].

RESULTS AND DISCUSSION

Molecular design

As shown in Fig. 1, the typical active N–N functionality embedded in pyridyl–pyrazole, pyridyl-pyrimidine and pyridyl-triazolopyrimidine will serve as a basic core ligand with a readily available metalation site. The designed molecule was synthesized using developed strategy reported earlier[38-40]. This incorporated imidazole and phenol features an installation of different biological application.

Fig. 1 Modifications of the piano stool complexes.

Synthesis and general aspects

In the ^{1}H NMR spectra of bipyrazoles, the pro-chiral methylene protons of pyrazoline appeared as two distinct doublets of a doublet, thereby indicating that both the protons are magnetically non-equivalent and diastereotopic. The chiral C–H proton of pyrazoline appeared as doublets of a doublet. In ^{1}H NMR of pyrimidin-2-amines, $–NH_2$ protons resonates as singlet at around δ 5.5-5.7 ppm. The aromatic protons resonate as multiples at around δ 6.00–8.00 ppm. The complexes of the type $[(\eta^5\text{-}C_5Me_5)Ir(L)]Cl$ (where L = bipyrazole; **7a-7b/**pyrimidin-2-amine; **8a-8b/**triazolopyrimidine; **9a-9b**) were prepared by addition of the chelating ligands to dichloromethane solution of $[\{(\eta^5\text{-}C_5Me_5)Ir(\mu\text{-}Cl)Cl\}_2]$ to form piano stool iridium^{III} complexes[41]. In the ^{1}H NMR spectra of complexes, the protons due to pro-chiral methylene protons resonated toward downfield side by difference of δ 0.5-1.5 ppm similarly the chiral C–H proton of pyrazoline and aromatic proton in complexes, resonated towards downfield side by difference of δ upto 1.0 and 0.5 ppm, respectively. It may be ascribed to the coordination of ligands to metal centre. The protons due to Cp*-CH_3 in complexes displayed an upfield shift and resonated at almost ~1.48 ppm with respect to the metal precursor complexes, which indicates a rather small change in the electronic environment about the metal centre. ^{13}C NMR spectral data of compounds further supported the formation of complexes and the proposed formulations (Supplementary material 1)[42-47]. The ESI-MS of complexes have been acquired to understand the relative composition and stability of the complexes. Notably these displayed the most abundant peaks for complex (7a) at m/z 808.37 $[M]^+$ and 810.43 $[M+2]^+$ (Supplementary material 2).

DNA binding by absorption spectral studies

There are a number of ways in which small molecules can interact with DNA. For example, groove binding, which is primarily an electrostatic interaction between a cationic molecule and the negative phosphate backbone of DNA. In covalent binding, a molecule coordinates to one of the base pairs of DNA (cis-platin covalently binds to DNA), and intercalation, resulting from insertion of the molecule or part of the molecule between the base pairs of DNA. Intercalation typically requires an extended flat aromatic group to accomplish this type of DNA interaction[48]. Because of the intense photophysical properties of metal complexes, a great deal of research has been conducted. In beginning with the initial studies by Barton and Turro in the mid-1980s[49, 50], associated with the development of ruthenium(II) complexes as DNA probes and phototherapeutics. To this end, we evaluated the interaction of iridium^{III} complexes with CT DNA by spectroscopic means[51-53]. The DNA binding experiment was performed in Tris-HCl buffer using DMSO solution of all compounds. The DNA concentration per nucleotide was determined by absorption spectroscopy using the molar absorption coefficient 6600 M^{-1} cm^{-1} at 260 and 280 nm A_{260}/A_{280} of 1.9, indicating that the DNA was sufficiently free of protein[54]. The stock solutions were stored at 4 ^{0}C and used within 4 days. Absorption titrations were carried out by varying the concentration of CT-DNA from 0 to 500 µL and with constant concentration of the compound (125 µL). In order to eliminate the absorbance of DNA itself; a reference cell containing DNA alone was prepared at the same concentration to which increments of the DNA stock solution were added. The binding of the ligands/complexes to DNA led to decrease in the absorption of the UV-Vis spectrum, indicating that the π^* orbital of the compounds can couple with the π orbital of the DNA base pairs, resulting in the decrease in the $\pi–\pi^*$ transition energy and causing a bathochromic shift. The binding constants (K_b) of the ligands/complexes to CT-DNA were determined by

monitoring the changes in the absorbance with increasing concentration of CT-DNA (Fig.2).

View Article Online
DOI: 10.1039/C6NJ02153K

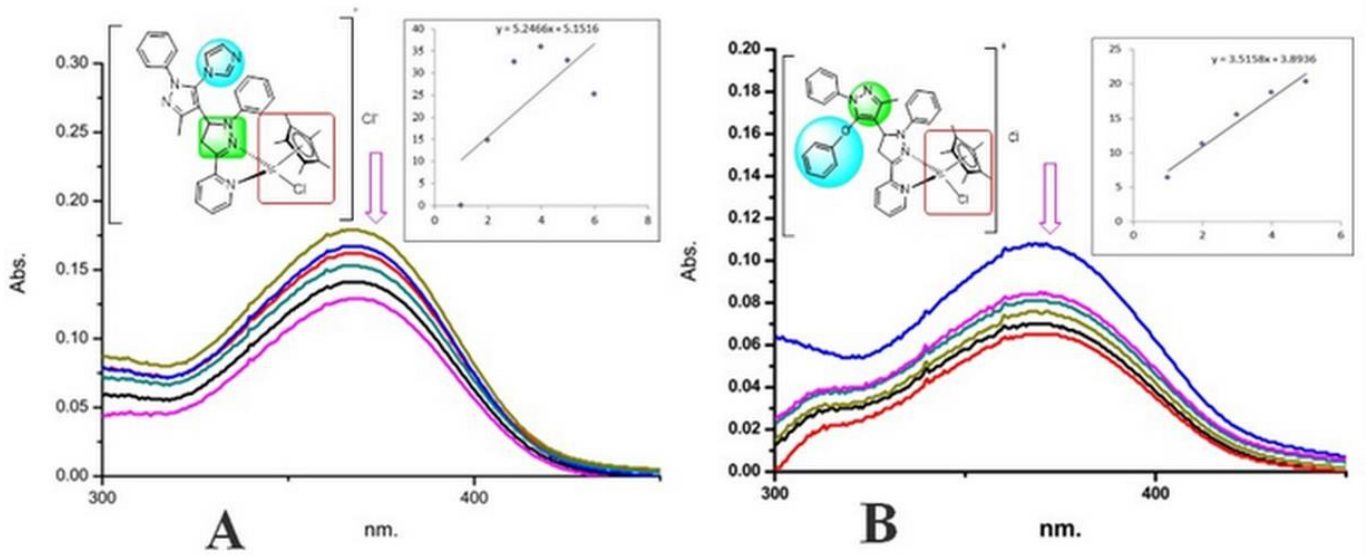

Fig. 2 (A) Absorption spectra of [(η^5-C_5Me_5)Ir(bpy-N)Cl]Cl (7a) (K_b = 1.13 ± 0.125 ×10^5 M^{-1}) with inset plot of [DNA]/(εa–εf) vs. [DNA]. Fig. 2 (B) Absorption spectra of [(η^5-C_5Me_5)Ir(bpy-O)Cl]Cl (7b) (K_b = 9.20 ± 0.049×10^4 M^{-1}) with inset plot of [DNA]/(εa–εf) vs. [DNA].

The absorption data were analysed to evaluate the intrinsic binding constant (K_b) determined from the spectroscopic titration data using the following equation.

$$[DNA]/(\varepsilon_a - \varepsilon_f) = [DNA]/(\varepsilon_b - \varepsilon_f) + 1/K_b\,(\varepsilon_b - \varepsilon_f)$$

The 'apparent' extinction coefficient (ε_a) was obtained by calculating absorbance of compounds. The terms ε_f and ε_b correspond to the extinction coefficients of free (unbound) and the fully bound ligands/complexes. The binding constant (K_b) was calculated using a plot inset (Fig. 2) of [DNA]/(ε_a - ε_f) *vs.* [DNA] from the ratio of slope to intercept[54]. In the present study, the heteroatom present in the ligands/complexes aromatic moiety can easily bind DNA base pairs[55]. The interaction of the complexes 7a and 7b with increase in calf thymus DNA is shown in Fig. 2. In the absorption spectrum, ligands and complexes exhibit more intense absorption bands, which are attributed to strong stacking interaction between the planar extended π-system, facilitating a non-covalent interaction of the compounds with the base pair of the DNA molecule[56, 57]. While increasing the concentration of the calf thymus DNA, the absorption band of the compounds is affected, this results in hypochromism and bathochromic (red) shift. The synthesized complexes 7a, 8a and 9a exhibit 25%, 32% and 30% of hypochromism, respectively and 3 nm, 5 nm and 5 nm of bathochromic shift, respectively, upon addition of DNA. The extent of hypochromism gives a measure of the strength of the intercalative binding. Results show that the compounds with imidazole substituent are better DNA binder as compared to the compounds having phenoxy substituent. The presence of the imidazole ring in the 7a, 8a and 9a is responsible for more hypochromism, indicating that the extent of interaction of compounds contain imidazole ring are stronger than that of others containing phenoxy substituent. The complexes 7a, 8a and 9a exhibit strong hydrophobic CT-DNA interaction due to the presence of an extended π-system of the aromatic imidazole ring and planarity of the molecule. The binding constant (K_b) of 7a, 8a and 9a with CT-DNA are found to be 1.13 ± 0.12[5] ×10^5, 1.51 ± 0.076 ×10^5 and 1.16 ± 0.085 ×10^5 M^{-1}, respectively. Which are found greater than rest of the complexes due to the presence of imidazole ring. Addition of calf thymus DNA to compounds show a decrease in absorbance of the π–π* band, which indicates that the binding of ligands and complexes with DNA are due to a strong interaction. The binding constant (K_b) values of the complexes are observed in the following order 8a > 9a > 7a > 8b > 7b > 9b. Table 1 shows the static binding constant of ligands and complexes with CT-DNA.

View Article Online
DOI: 10.1039/C6NJ02153K

Table 1: Absorption spectral properties of ligands and Ir^{III} complexes bound to CT DNA presented with standard deviation for three independent experiments.

Compounds	Wavelength	Shift	% Hypochromism	Binding constant (K_b) × 10^5 (M^{-1})
4a	375	2	12±1.5	0.35±0.027
4b	379	2	11±0.6	0.14±0.023
5a	265	2	12±1.2	0.43±0.020
5b	268	3	13±1.0	0.26±0.008
6a	314	2	16±0.6	0.58±0.012
6b	316	3	15±0.6	0.48±0.008
7a	367	3	25±1.0	1.13±0.125
7b	368	4	22±1.0	0.92±0.049
8a	399	5	32±6.1	1.51±0.076
8b	380	5	24±1.2	0.94±0.016
9a	398	5	30±1.0	1.16±0.085
9b	409	4	17±1.2	0.51±0.013

Molecular docking of the complexes with the DNA duplex with sequence d(CGCGAATTCGCG)$_2$

In addition to the wet lab activity, we have also performed the computational work (molecular docking) for all synthesized compounds (Supplementary material 4). Molecular docking of the complexes with the DNA duplex with sequence d(ACCGACGTCGGT)$_2$. The molecular docking technique has played important roles in understanding the drug–DNA interactions for the rational drug design and discovery, as well as in the mechanistic study by placing a small molecule in the binding site of the target specific region of the DNA mainly in a non-covalent fashion.[58] Docking was performed to preliminarily predict the binding affinity and the chosen binding site along with the sterically acceptable conformations. It is generally accepted that the lower the binding free energy, the more potent the binding affinity is between the receptor (DNA) and ''the ligand'' molecules. Amongst all possible conformation, a structure having the most optimal energy was chosen for the final binding orientation analysis (supplementary material 3).

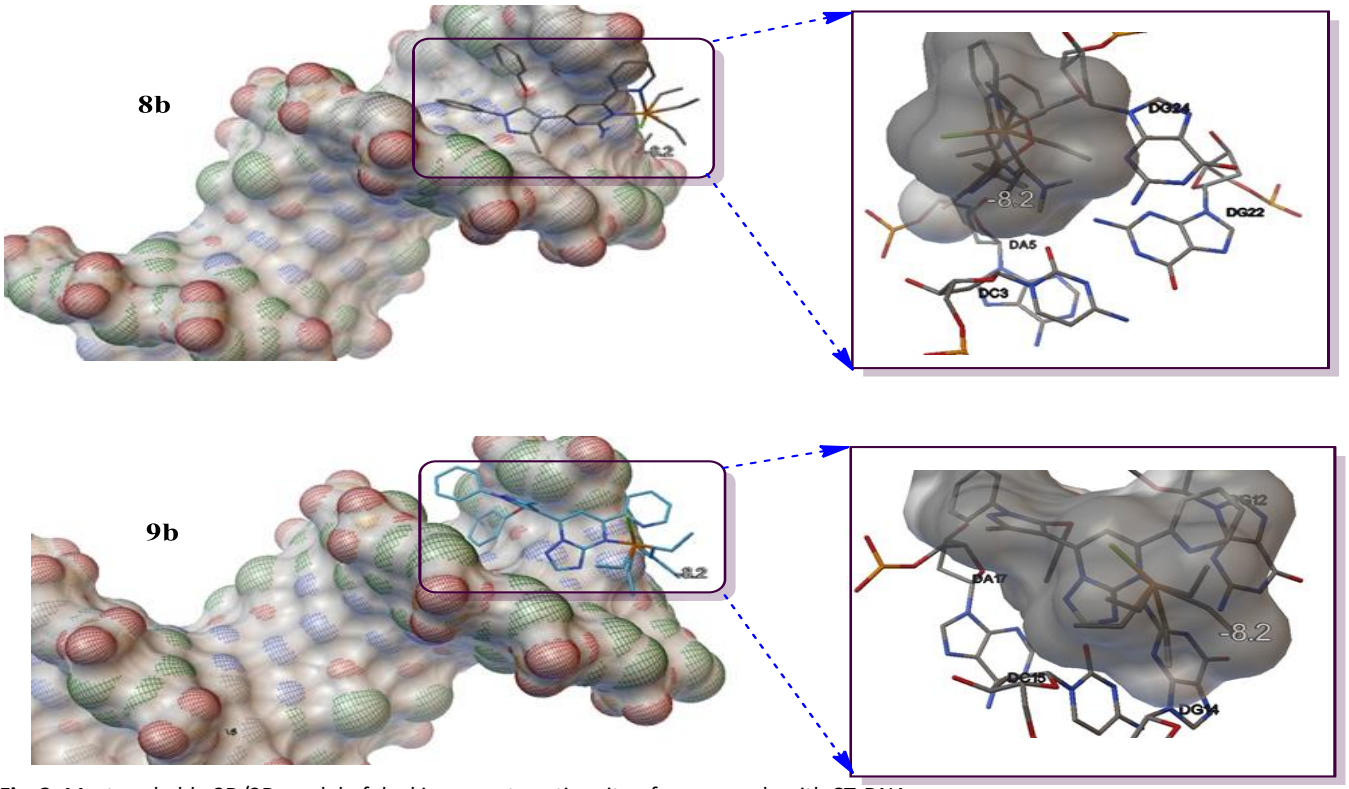

Fig. 3: Most probable 2D/3D model of docking pose to active site of compounds with CT-DNA

View Article Online
DOI: 10.1039/C6NJ02153K

Journal Name

ARTICLE

Table 2: Molecular docking results of in terms of glide docking score (kcal mol^{-1})

Compounds	Glide docking score	Compounds	Glide docking score
4a	-6.7	7a	-8.1
4b	-7.0	7b	-8.0
5a	-7.2	8a	-7.2
5b	-7.5	8b	-8.2
6a	-7.3	9a	-8.0
6b	-7.4	9b	-8.2

The docked pose with minimum energy clearly showed that minor groove mode played a predominant role in the interaction. As can be seen from the Docking score,[59, 60] listed in Table 2. The negative values of the binding free energy of docked complexes suggest that the compounds reasonably bind to the DNA. The complex 8b stacked between DG24 and DG22 of chain A and DC3 and DA5 of chain B. The complex 9b stacked between DG12 of chain A and DG14, DC15 and DA17 of chain B. The complexes 8b and 9b are having a good interaction with the receptor (Fig. 3). From the resulting docked structures it is clear that compounds fit well into the minor groove of the targeted DNA and G–C rich region, stabilized by van der Waals interactions and hydrophobic contacts.

Chemical nuclease activity

The activity of the complexes as chemical nucleases was studied using supercoiled pUC19 DNA in 1% agarose gel at 100 V for 2 h. The efficiency of the complexes was compared with that of the ligands and dimer under the same conditions. The DNA cleavage can occur by hydrolytic and oxidative pathways[61], in which hydrolytic DNA cleavage involves cleavage of phosphodiester bond to generate fragments and converting supercoil (SC) form of DNA to open-circular (OC) form and last in linear (L) form[62], is being used for identifying the percentage of cleavage as a function of concentration of nuclease. Oxidative DNA cleavage involves either oxidation of the deoxyribose moiety by abstraction of sugar hydrogen or oxidation of nucleobases[63].

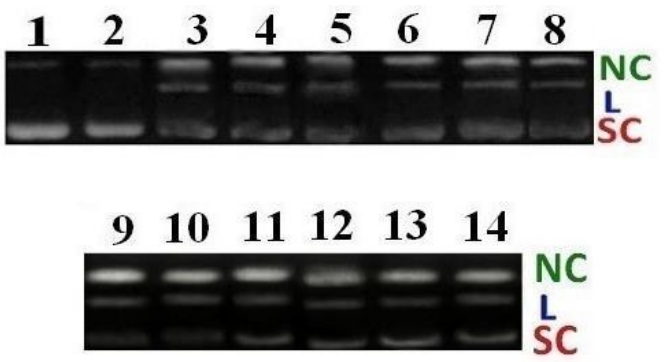

Fig. 4: Cleavage of SC pUC19 DNA with series of ligands and complexes (50 µM) using 1% agarose gel containing 0.5 µg/mL ethidium bromide. All reactions were incubated in TE buffer (pH 8) in a final volume of 20 µL, for 24 h. at 37 °C. Lane 1, DNA control; Lane 2, DNA+dimer; Lane 3-4, DNA+(4a-4b); Lane 5-6, DNA+(5a-5b); Lane 7-8, DNA+(6a-6b); Lane 9-10, DNA+(7a-7b); Lane 11-12, DNA+(8a-8b); Lane 13-14, DNA+(9a-9b); Abbreviations: N = nicked; S = supercoiled; L= linear.

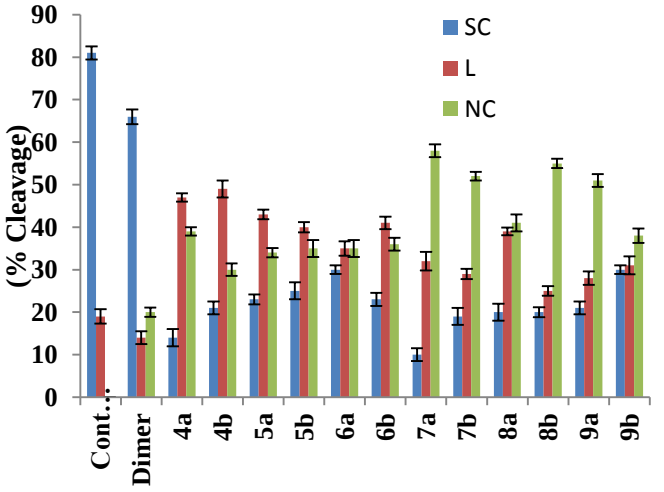

Fig. 5: Percentage cleavage of SC, NC and linear form of DNA presented with standard deviation for three independent experiments.

The principle of this method is that molecules migrate in the gel as a function of their mass, charge and shape. The supercoiled DNA, migrating faster than open circular molecules of the same mass and charge. The native DNA remains in the supercoiled (SC) form. Single strand cleavage results in so called nicked (NC) or open circular (OC) form of DNA whereas the double-strand cleavage results in linear form of DNA. The migration rate during agarose gel electrophoresis depends on both size (base pairs) and conformation, with smaller or condensed DNA migrating faster than larger or unfolded DNA. SC has a tightly packed

View Article Online
DOI: 10.1039/C6NJ02153K

conformation and therefore migrates faster through agarose gels than linear DNA (intermediate migration) or open circle DNA (slowest migration)[64]. Results show that all complexes are better DNA cleaving agents as compared to ligands and salt as well. Complexes 7a and 7b induce almost degradation of DNA, 90% and 86%, respectively. The pertinent cleavage data are presented in supplementary material 4.

Antiproliferative activity

The antiproliferative activity of ligands and complexes in A549 (lung) cancer cells have been shown in Fig. 6. The ligand 5b (phenoxy substituted pyrimidin-2-amine) shows excellent anticancer activity than other synthesized ligands. All the synthesized complexes are found better anticancer agents as compared to ligands (supplementary material 5). The complexes having ether linkage are more potent than complexes having N –linkage. The complexes of pyrimidin-2-amine i.e. 8a and 8b exhibit better activity as compared to complexes of bipyrazole and triazolopyrimidine. This proves that compounds of pyrimidin-2-amine are most potent than pyrazole or fused triazolopyrimidine. The anticancer activity of complexes are in order of **7a < 9a < 9b < 8a < 7b < 8b.** Synthesized complexes exhibit better anticancer activity than previously reported half-sandwich pentamethylcyclopentadienyl iridium^{III} complexes (IC_{50} = 1-89 µM[66]) and iridium-Cp* chloride picolinamide complexes (IC_{50} = 30-190 µM[67]).

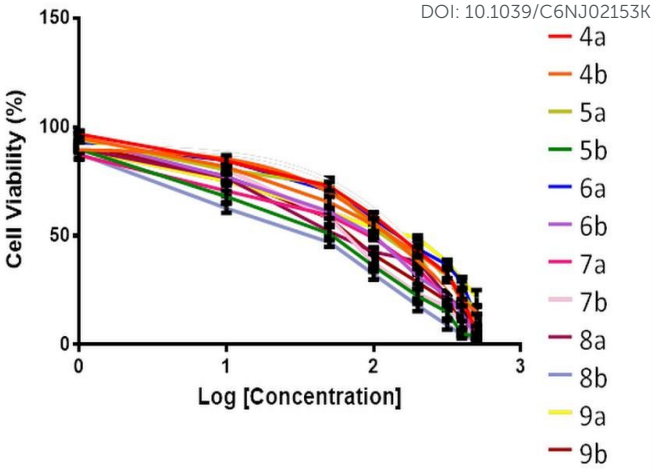

Fig. 6: Cell viability assay presented in percentage with standard deviation for three independent experiments.

***In vitro* antibacterial activity**

The antimicrobial activities of all newly synthesized bipyrazole, pyrimidin-2-amine and triazolopyrimidines derivatives were tested against arbitrarily selected two Gram positive and three Gram negative bacterial strains. When tested for antibacterial activity, cyclopentadienyl dimer has been found to be inactive. Thus, oxidative stress by iridium seems to enhance antibacterial potency but is not the only component determining antibiotic activity. The aim was to incorporate pyrazole on iridium to check the antibiotic activity. So, we synthesized pyrazole incorporatedbipyrazoles/pyrimidin-2-amines/ triazolopyrimidines. When tested for antibacterial activity of 6a and 6b, they exhibit good results compared to rest with MIC values in the range of 248–267 µM (Fig.7). These results suggest that neither iridium dimer nor pyrazole based ligands are found active as an individual, but the coordination of both is indispensable for antibacterial activity demonstrating that the organometallic moiety alone is not sufficient for antibiotic activity but needs the pyrazole based backbone. A satisfactory reason for this increase in antibacterial activity may be considered in the light of Overtone's concept[30] and chelation theory.

View Article Online
DOI: 10.1039/C6NJ02153K

Journal Name

ARTICLE

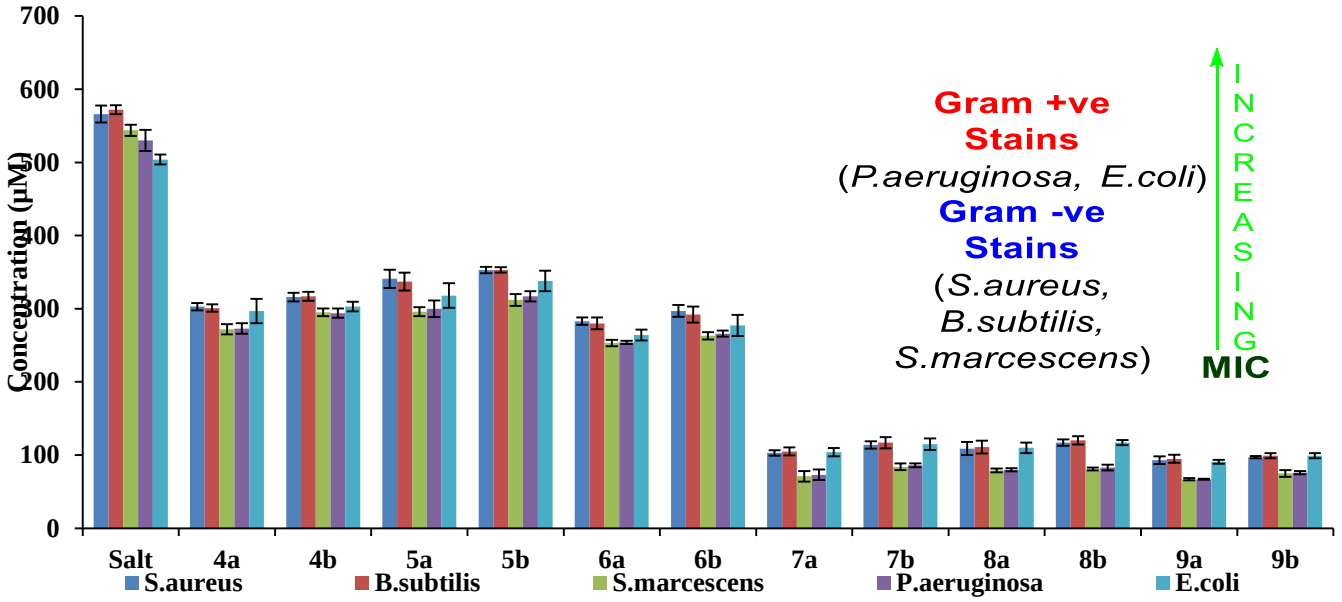

Fig. 7: The antimicrobial activity results in µM presented with standard deviation for three independent experiments.

According to Overtone's concept of cell permeability, the lipid membrane that surrounds cell favours the passage of only lipid soluble materials. As a consequence of that the liposolubility is an important factor which controls bacteriostatic activity. On chelation, the polarity of the Ir^{III} ion will be lowered to a greater extent due to the overlap of the ligand orbital and partial sharing of the positive charge of the Ir^{III} ion with donor groups. Further, it increases the delocalization of π- electrons over whole chelate ring and enhances lipophilicity of the complexes. This increased lipophilicity, enhances the penetration of the complexes into lipid membranes and blocks the metal binding sites in bacterial enzymes. The complexes also disturb the respiratory processes of the cell and thus block the synthesis of proteins, which restricts further growth of the organism. The antibacterial activity was evaluated by minimal inhibitory concentration (MIC) values. The pertinent MIC data are presented in supplementary material 6. The purely organic intermediate compounds were inactive at some extent whilst upon chelation they proved better antimicrobial agents (70-125 µM). It is worth mentioning that compounds showed lower activity against Gram positive bacteria. This might be due to the presence of the outer membrane of Gram positive bacteria, which hinders access of many compounds to the cytoplasmic membrane where complexes exert its activity.

Cytotoxicity on brine shrimp

All the synthesized compounds were screened for their cytotoxicity (brine shrimp bioassay) using the protocol of Meyer et al[35]. Brine shrimp lethality bioassay is a development in the assay procedure of bioactive compound, which indicates cytotoxicity as well as a wide range of pharmacological activities of the compounds. Results for the lethality were noted in terms of deaths of larvae. The mortality rate of brine shrimp nauplii was found to increase with increasing the concentration of complexes. A plot of the log of sample's concentration versus percentage of mortality showed a linear correlation. From the graph, the LC_{50} values of the compounds were calculated and it is observed from the results (Fig.8) that **6a** and **6b** proved to be good cytotoxic agents (5.0 ± 0.032 µM and 5.34 ± 0.059 µM, respectively) as compared to all other ligands.

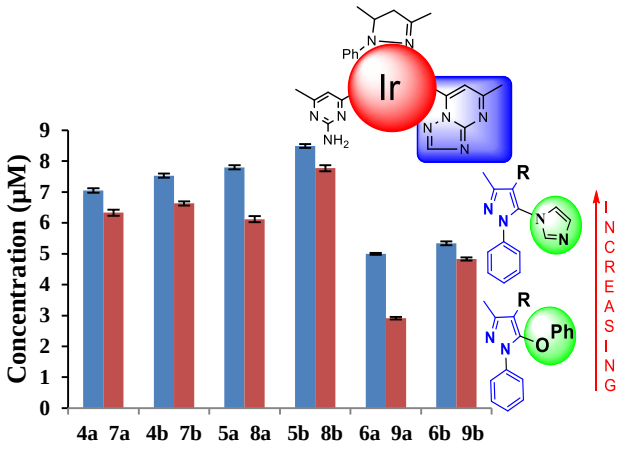

Fig. 8: Influence of the compounds on the brine shrimp lethality bioassay presented with standard deviation for three independent experiments.

It indicates that the triazolopyrimidines are more cytotoxic than that of pyrazolines and pyrimidin-2-amine. The compounds containing imidazole nucleus are more potent than that of phenoxy nucleus substituted at 5th position on 1-phenyl-3-methyl-pyrazole. The order of potency of pyrazole incorporated compounds is **5b < 5a < 8b < 4b < 4a < 7b < 8a < 7a < 6b < 6a < 9b < 9a.** The tested Ir^{III} complexes have strong cytotoxic activity but this examination is a primary one and further tests are required to investigate its actual mechanism of cytotoxicity and its probable effects on higher animal model and on cancer cell line. The pertinent cytotoxic data are presented in supplementary material 7.

Cytotoxicity on *S. pombe*

In the present study, *S. pombe* cells have been used to study cytotoxic effect of compounds at a cellular level. *S. pombe* cells has become an important tool to study cell biology due to its eukaryotic and fairly big size characteristics. A comparative study of cellular level cytotoxicity values of the free ligands and their complexes indicate that the metal complexes show better activity against *S. pombe* cells compared to the pyrazole incorporated ligands. Cell death caused by toxicity of the chemically synthesized compounds could be easily monitored by vital staining (Fig.9).

View Article Online
DOI: 10.1039/C6NJ02153K

Fig. 9: Effect of compounds on *S. pombe* cells, dead cells are seen dark whereas live cells are seen transparent.

The toxicity was found to vary with the type of substituent, principal moieties and concentrations of the synthesized compounds. General observation is that as concentration of compounds increases the cytotoxicity is also increases[37]. After treatment, many of the *S. pombe* cells are killed due to toxic nature of the compound. From Table 3, we observed that the cytotoxicity activity of Ir^{III} complexes found better than that of respective free ligands. The order of potency of compounds is complexes > triazolopyrimidines > pyrazolines > pyrimidin-2-amines. The compounds bearing imidazole ring show better results than rest of all. 6a is more potent amongst all ligands and complex 9a is most toxic amongst all synthesized compounds.

Table 3: Percentage viability on *S.pombe* cells presented with standard deviation for three independent experiments.

Compounds	% Viability per concentration				
	2 μM	4 μM	6 μM	8 μM	10 μM
4a	81	76	70	65	61
4b	83	78	71	67	62
5a	82	77	72	66	63
5b	85	80	74	69	65
6a	79	74	68	63	59
6b	81	76	70	65	61
7a	65	60	54	49	45
7b	67	62	56	51	47
8a	66	62	58	53	49
8b	69	64	58	53	49
9a	63	57	52	47`	43
9b	65	60	54	49	45

CONCLUSION

In conclusion, the biological and medicinal chemistry of $iridium^{III}$ complexes has been little explored previously, perhaps because it is often assumed that low-spin $5d^6$ Ir^{III} complexes are highly kinetically inert. Our data show that this is not always the case. The cyclopentadienyl ligands, while stabilizing Ir^{III}, can confer kinetic labile ligands such as chloride. Moreover, pyrazole based

heterocyclic frameworks can have a major effect on the chemical and biological behaviour of $[(\eta^5\text{-Cp}^*)\text{Ir(XY)Cl}]^+$ complexes. This appears to be the first time that bipyrazole/pyrimidin-2-amine/triazolopyrimidine ligands have been used in iridium^{III} complexes. In general, the introduction of pyrazole based ligands to iridium^{III} enhances its activity against brine shrimp and *S. pombe.* The complexes of triazolo[1,5-a]pyrimidines are proven to be most cytotoxic. The chelating ligands and metal complexes appear to determine the selectivity of nucleobases binding. The complexes containing imidazole in N, N-chelating ligands stack strongly between the base pairs of CT DNA, in contrast the complexes containing phenoxy shows poor binding. Furthermore, the complexes 7b and 8b are found excellent anticancer agent as compared to some previous reported literature, this is because of the presence of phenoxy substituent on pyrazole ring as compared to imidazole substituent. In addition Ir^{III} complexes show amended inhibition against bacterial species as compared to ligands that is also supported by DNA cleavage data. The work reported here demonstrates that rational chemical design can be applied to Ir^{III} complexes to achieve potent biological activity. It is notable that pyrazole substituents can also play a major role in controlling the chemical and biological properties of metal complexes. In general, iridium complexes offer much promise for the design of novel therapeutic agents.

ACKNOWLEDGMENTS

This work was supported by UGC, New Delhi for providing BSR-one time grant fellowship and UGC-BSR JRF/SRF 5/100. The authors thank the Head, Department of Chemistry, Sardar Patel University for providing research facilities and CISST, Vallabh Vidyanagar for LC-MS. Authors are thankful to P. D. Patel Institute of applied sciences for providing cell culture facilities.

REFERENCES

1. C. Shobha Devi, P. Nagababu, S. Natarajan, N. Deepika, P. Venkat Reddy, N. Veerababu, S. S. Singh and S. Satyanarayana, *Eur. J. Med. Chem.*, 2014, **72**, 160-169.
2. M. Chauhan, K. Banerjee and F. Arjmand, *Inorg. Chem.*, 2007, **46**, 3072-3082.
3. Y. Sun, S. Bi, D. Song, C. Qiao, D. Mu and H. Zhang, *Sensors Actuators B: Chem.*, 2008, **129**, 799-810.
4. F. M. Foley, F. R. Keene and J. G. Collins, *J. Chem. Soc., Dalton Trans.*, 2001, 2968-2974.
5. C.-W. Jiang, *J. Inorg. Biochem.*, 2004, **98**, 497-501.
6. O. Van Gijte and A. Kirsch-De Mesmaeker, *J. Chem. Soc., Dalton Trans.*, 1999, 951-956.
7. E. Wong and C. M. Giandomenico, *Chem. Rev.*, 1999, **99**, 2451-2466.
8. E. R. Jamieson and S. J. Lippard, *Chem. Rev.*, 1999, **99**, 2467-2498.
9. L. Kelland, *Nat Rev Cancer*, 2007, **7**, 573-584.
10. D. Wang and S. J. Lippard, *Nat Rev Drug Discov*, 2005, **4**, 307-320.
11. C. G. Hartinger and P. J. Dyson, *Chem. Soc. Rev.*, 2009, **38**, 391-401. View Article Online DOI: 10.1039/C6NJ02153K
12. R. H. Fish and G. Jaouen, *Organometallics*, 2003, **22**, 2166-2177.
13. Y. K. Yan, M. Melchart, A. Habtemariam and P. J. Sadler, *Chem. Commun.*, 2005, 4764-4776.
14. G. Suss-Fink, *Dalton Transactions*, 2010, **39**, 1673-1688.
15. B. T. Loughrey, P. C. Healy, P. G. Parsons and M. L. Williams, *Inorg. Chem.*, 2008, **47**, 8589-8591.
16. M. G. Mendoza-Ferri, C. G. Hartinger, M. A. Mendoza, M. Groessl, A. E. Egger, R. E. Eichinger, J. B. Mangrum, N. P. Farrell, M. Maruszak, P. J. Bednarski, F. Klein, M. A. Jakupec, A. A. Nazarov, K. Severin and B. K. Keppler, *J. Med. Chem.*, 2009, **52**, 916-925.
17. R. E. Aird, J. Cummings, A. A. Ritchie, M. Muir, R. E. Morris, H. Chen, P. J. Sadler and D. I. Jodrell, *Br. J. Cancer*, 2002, **86**, 1652-1657.
18. P. A. H. Lay and W. D., *In Advances in Inorganic Chemistry;*, Academic Press: New York, 1991.
19. D. T. Richens, *Chem. Rev.*, 2005, **105**, 1961-2002.
20. L. Helm and A. E. Merbach, *Coord. Chem. Rev.*, 1999, **187**, 151-181.
21. G. Sava, T. Giraldi, G. Mestroni and G. Zassinovich, *Chem.-Biol. Interact.*, 1983, **45**, 1-6.
22. M. J. Cleare, *Coord. Chem. Rev.*, 1974, **12**, 349-405.
23. H. Amouri, J. Moussa, A. K. Renfrew, P. J. Dyson, M. N. Rager and L.-M. Chamoreau, *Angew. Chem. Int. Ed.*, 2010, **49**, 7530-7533.
24. C. G. Hartinger, *Angew. Chem. Int. Ed.*, 2010, **49**, 8304-8305.
25. F. Shao and J. K. Barton, *J. Am. Chem. Soc.*, 2007, **129**, 14733-14738.
26. A. Wilbuer, D. H. Vlecken, D. J. Schmitz, K. Kräling, K. Harms, C. P. Bagowski and E. Meggers, *Angew. Chem. Int. Ed.*, 2010, **49**, 3839-3842.
27. L. Messori, G. Marcon, P. Orioli, M. Fontani, P. Zanello, A. Bergamo, G. Sava and P. Mura, *J. Inorg. Biochem.*, 2003, **95**, 37-46.
28. G. Marcon, A. Casini, P. Mura, L. Messori, A. Bergamo and P. Orioli, *Met.-Based Drugs*, 2000, **7**, 195-200.
29. S. Ramakrishnan, E. Suresh, A. Riyasdeen, M. A. Akbarsha and M. Palaniandavar, *Dalton Transactions*, 2011, **40**, 3245-3256.
30. S. B. Gajera, J. V. Mehta and M. N. Patel, *RSC Advances*, 2015, **5**, 21710-21719.
31. P. P. Yadav, P. Gupta, A. K. Chaturvedi, P. K. Shukla and R. Maurya, *Biorg. Med. Chem.*, 2005, **13**, 1497-1505.
32. M. Patra, M. Wenzel, P. Prochnow, V. Pierroz, G. Gasser, J. E. Bandow and N. Metzler-Nolte, *Chemical Science*, 2015, **6**, 214-224.
33. A. K. Sadana, Y. Mirza, K. R. Aneja and O. Prakash, *Eur. J. Med. Chem.*, 2003, **38**, 533-536.
34. D. J. Finney, *Cambridge University Press*, 1971.
35. B. N. Meyer, N. R. Ferrigni, J. E. Putnam, L. B. Jacobsen, D. E. Nichols and J. L. McLaughlin, *Planta Med.*, 1982, **45**, 31-34.
36. J. V. Mehta, S. B. Gajera and M. N. Patel, *Spectrochimica Acta Part A: Molecular and Biomolecular Spectroscopy*, 2015, **136, Part C**, 1881-1892.

37. J. V. Mehta, S. B. Gajera, P. Thakor, V. R. Thakkar and M. N. Patel, *RSC Advances*, 2015, **5**, 85350-85362.
38. P. Kaswan, K. Pericherla, D. Purohit and A. Kumar, *Tetrahedron Lett.*, 2015, **56**, 549-553.
39. K. M. Amin, M. M. Kamel, M. M. Anwar, M. Khedr and Y. M. Syam, *Eur. J. Med. Chem.*, 2010, **45**, 2117-2131.
40. M. Sharma, V. Chaturvedi, Y. K. Manju, S. Bhatnagar, K. Srivastava, S. K. Puri and P. M. S. Chauhan, *Eur. J. Med. Chem.*, 2009, **44**, 2081-2091.
41. C. P. Casey, J. M. O'Connor, W. D. Jones and K. J. Haller, *Organometallics*, 1983, **2**, 535-538.
42. S. R. Halper and S. M. Cohen, *Angew. Chem. Int. Ed.*, 2004, **43**, 2385-2388.
43. D. L. Murphy, M. R. Malachowski, C. F. Campana and S. M. Cohen, *Chem. Commun.*, 2005, 5506-5508.
44. T. E. Wood and A. Thompson, *Chem. Rev.*, 2007, **107**, 1831-1861.
45. S. A. Baudron, *CrystEngComm*, 2010, **12**, 2288-2295.
46. J. D. Hall, T. M. McLean, S. J. Smalley, M. R. Waterland and S. G. Telfer, *Dalton Transactions*, 2010, **39**, 437-445.
47. D. Salazar-Mendoza, S. A. Baudron and M. W. Hosseini, *Inorg. Chem.*, 2008, **47**, 766-768.
48. A. Wolfe, G. H. Shimer and T. Meehan, *Biochemistry (Mosc).* 1987, **26**, 6392-6396.
49. J. K. Barton, J. M. Goldberg, C. V. Kumar and N. J. Turro, *J. Am. Chem. Soc.*, 1986, **108**, 2081-2088.
50. C. V. Kumar, J. K. Barton and N. J. Turro, *J. Am. Chem. Soc.*, 1985, **107**, 5518-5523.
51. A. E. Friedman, J. C. Chambron, J. P. Sauvage, N. J. Turro and J. K. Barton, *J. Am. Chem. Soc.*, 1990, **112**, 4960-4962.
52. P. Nagababu, A. K. Barui, B. Thulasiram, C. S. Devi, S. Satyanarayana, C. R. Patra and B. Sreedhar, *J. Med. Chem.*, 2015, **58**, 5226-5241.
53. S. Swavey, M. DeBeer and K. Li, *Inorg. Chem.*, 2015, **54**, 3139-3147.
54. P. R. Reddy, A. Shilpa, N. Raju and P. Raghavaiah, *J. Inorg. Biochem.*, 2011, **105**, 1603-1612.
55. P. Uma Maheswari, V. Rajendiran, H. Stoeckli-Evans and M. Palaniandavar, *Inorg. Chem.*, 2006, **45**, 37-50.
56. C. Zhang, Z. Wang, S. Song, X. Meng, Y.-S. Zheng, X.-L. Yang and H.-B. Xu, *The Journal of Organic Chemistry*, 2014, **79**, 2729-2732.
57. S. Ramakrishnan and M. Palaniandavar, *Dalton Transactions*, 2008, 3866-3878.
58. G. M. Morris, D. S. Goodsell, R. S. Halliday, R. Huey, W. E. Hart, R. K. Belew and A. J. Olson, *J. Comput. Chem.*, 1998, **19**, 1639-1662.
59. S. Mukhopadhyay, R. K. Gupta, R. P. Paitandi, N. K. Rana, G. Sharma, B. Koch, L. K. Rana, M. S. Hundal and D. S. Pandey, *Organometallics*, 2015, **34**, 4491-4506.
60. K. Rajavelu and P. Rajakumar, *Journal of Materials Chemistry B*, 2015, **3**, 3340-3350.
61. B. Maity, M. Roy, B. Banik, R. Majumdar, R. R. Dighe and A. R. Chakravarty, *Organometallics*, 2010, **29**, 3632-3641.
62. S. Ramakrishnan, V. Rajendiran, M. Palaniandavar, V. S. Periasamy, B. S. Srinag, H. Krishnamurthy and M. A. Akbarsha, *Inorg. Chem.*, 2009, **48**, 1309-1322.
63. S. Roy, S. Saha, R. Majumdar, R. R. Dighe and A. R. Chakravarty, *Inorg. Chem.*, 2009, **48**, 9501-9509.
64. P. Kumar, S. Gorai, M. Kumar Santra, B. Mondal and D. Manna, *Dalton Transactions*, 2012, **41**, 7573-7581.
65. Z. Liu, I. Romero-Canelón, A. Habtemariam, G. J. Clarkson and P. J. Sadler, *Organometallics*, 2014, **33**, 5324-5333.
66. A. J. Millett, A. Habtemariam, I. Romero-Canelón, G. J. Clarkson and P. J. Sadler, *Organometallics*, 2015, **34**, 2683-2694.
67. Z. Almodares, S. J. Lucas, B. D. Crossley, A. M. Basri, C. M. Pask, A. J. Hebden, R. M. Phillips and P. C. McGowan, *Inorganic Chemistry*, 2014, **53**, 727-736.

View Article Online
DOI: 10.1039/C6NJ02153K

Table of Contents Graphic:

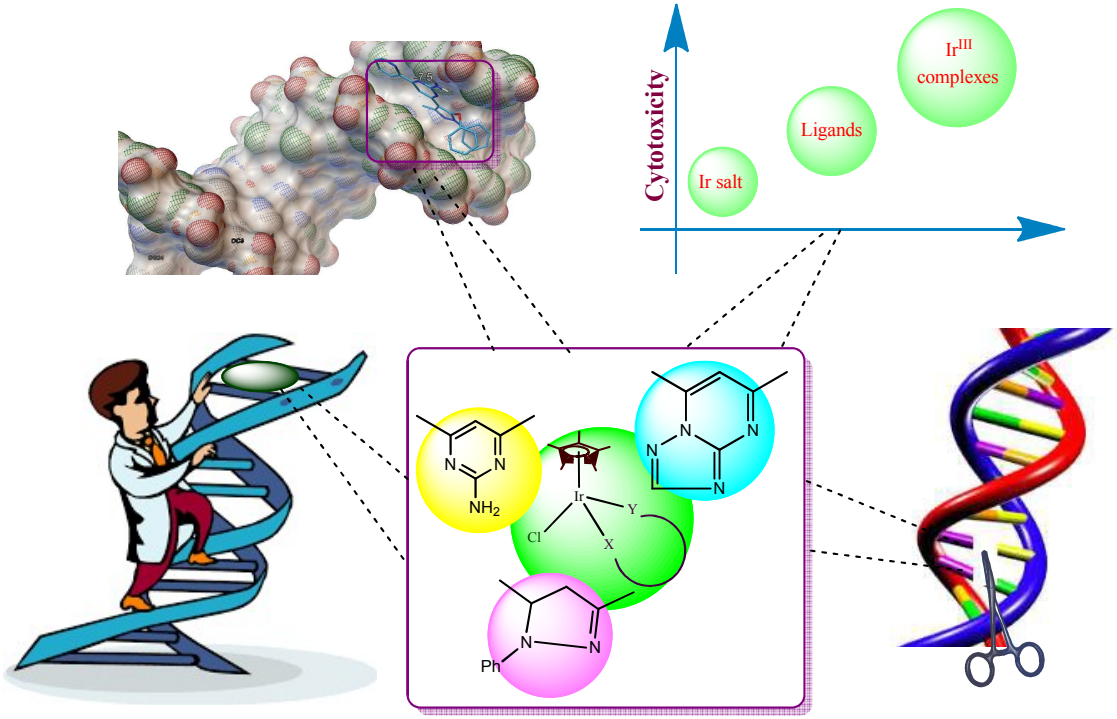

Table of Contents synopsis:

Enhancement in the biological function i.e., DNA binding, molecular docking, Antiproliferative and DNA cleavage of metal complexes as compared to free ligands.